情報計測処理論
「太陽系探査データ処理」
Analysis of solar system exploration data

新領域創成科学研究科　複雑理工学専攻
今村　剛

Remote sensing in planetary exploration

- Radio wave measurement
  - Doppler measurement of spacecraft signals
  - Spectroscopy
  - Radar sounding
  - Radio interferometry (e.g, SAR, VLBI)

- Optical (short wavelength EM wave) measurement
  - Imaging
  - Spectroscopy
  - Laser sounding

Radio occultation measurement

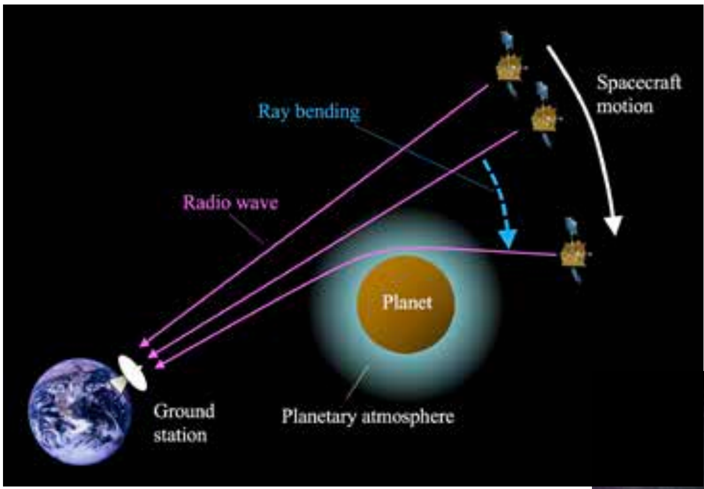

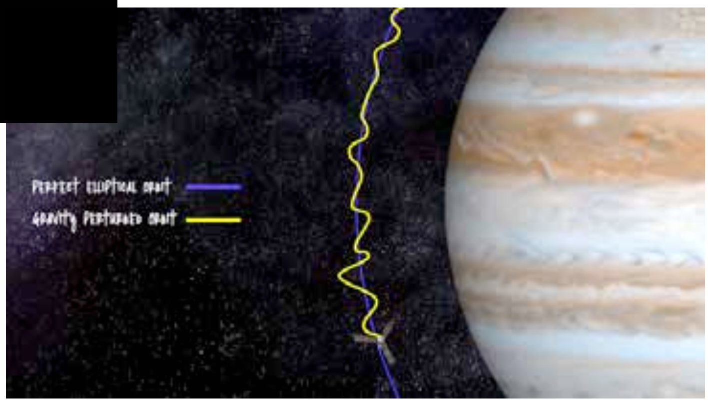

Observation of gravity anomaly by Doppler tracking of spacecraft (NASA's Juno)

Vertical temperature profiles of planetary atmospheres

(Mueller-Wodarg et al.)

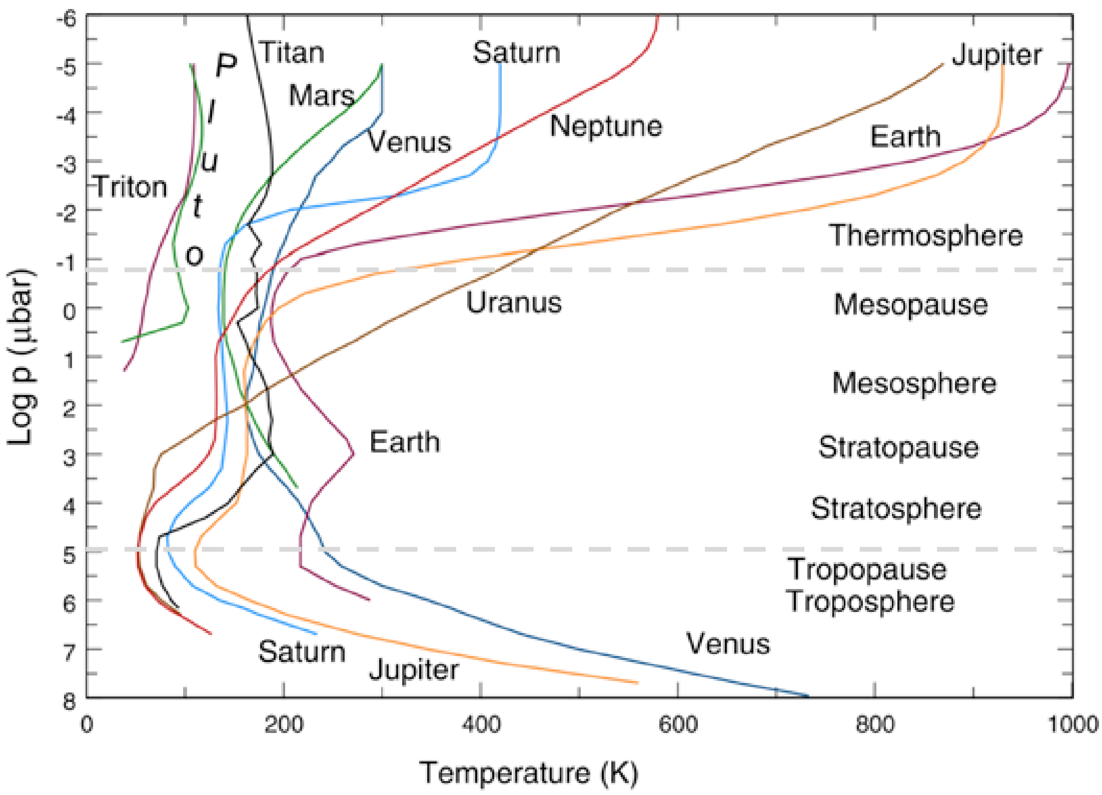

Radio occultation measurement

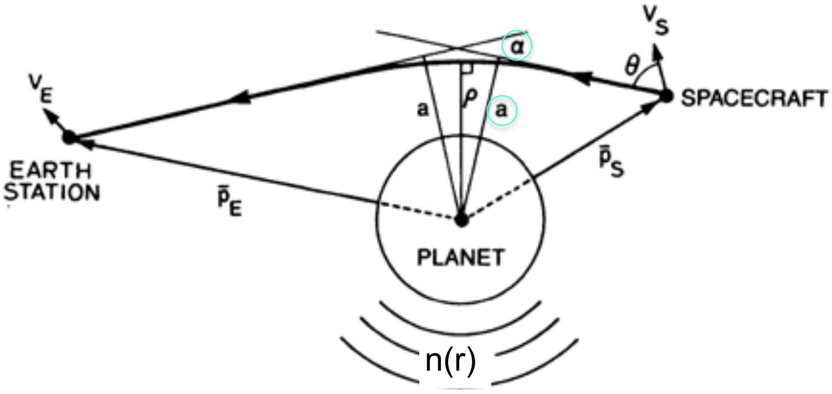

a : Impact parameter
α : Bending angle
n : Refractive index
r : Distance from planet center

Tyler (1987)

$$\alpha(a) = -2a \int_{r=r_0}^{r=\infty} \frac{1}{n} \frac{\partial n}{\partial r} \frac{dr}{\sqrt{(nr)^2 - a^2}}$$

Abel transformation:

$$\pi \ln n(r_{01}) = -\int_{a=a_1}^{a=\infty} \frac{\alpha(a)}{\sqrt{a^2 - a_1^2}} da$$

Retrieval of a temperature profile (Venus orbiter Akatsuki)

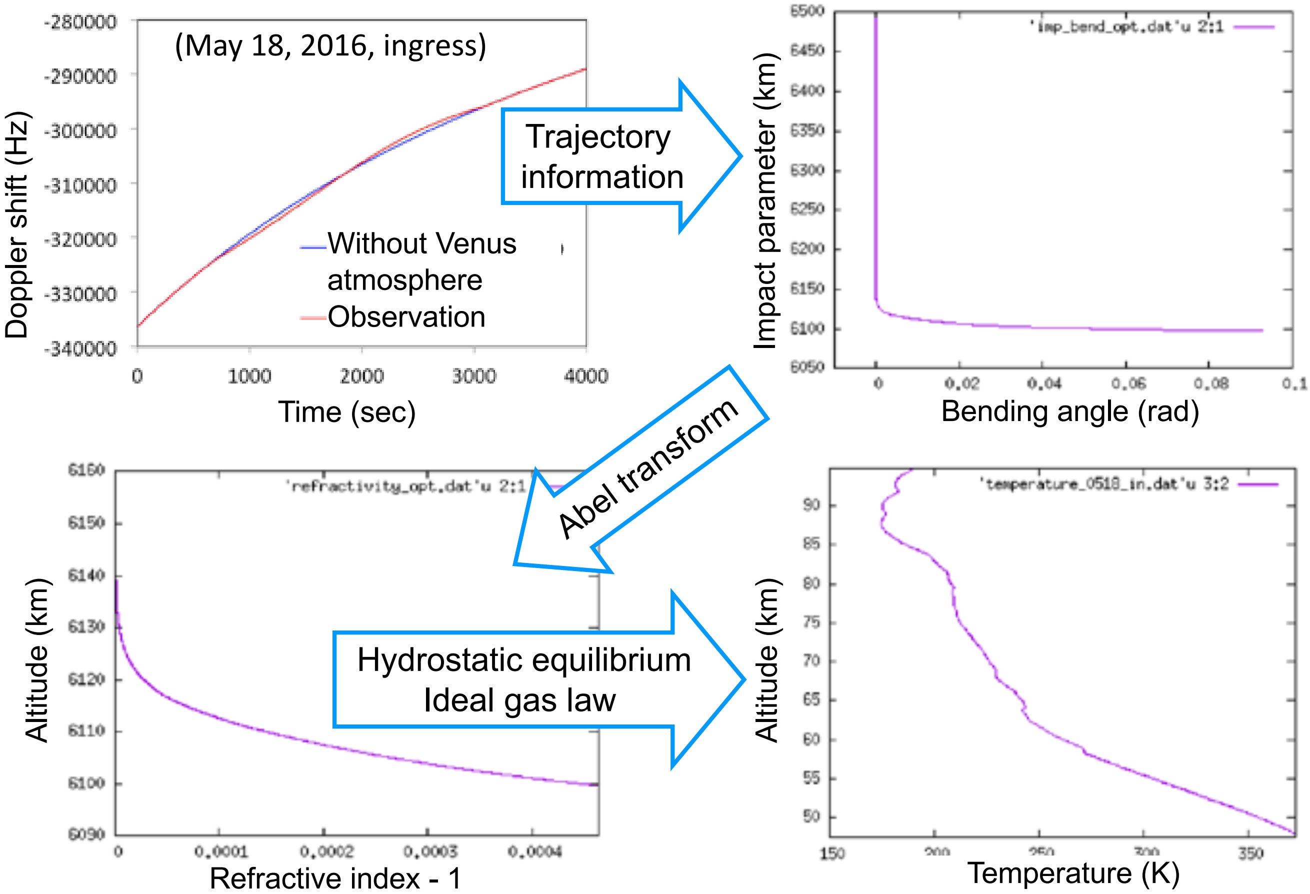

Required accuracy

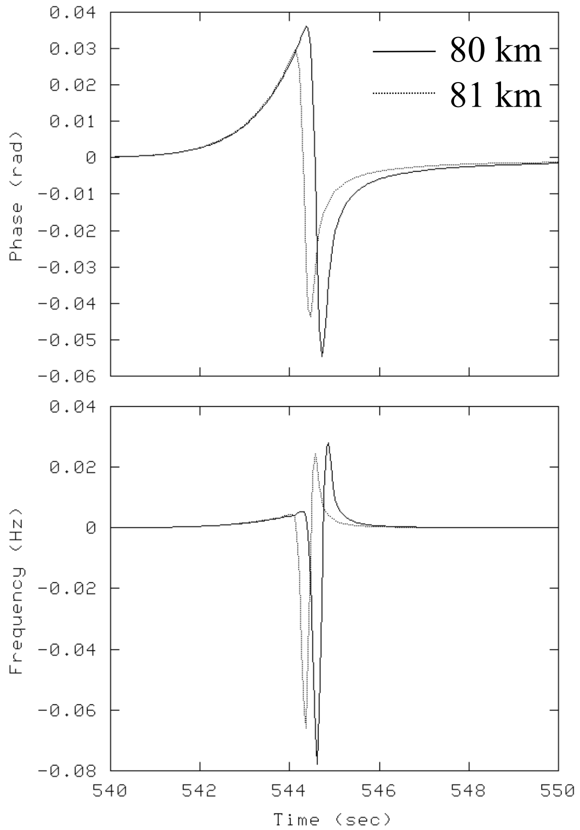

Change in phase/frequency caused by a Gaussian-type 0.2 K-perturbation with 1 km-thickness

Transmit frequency ~ 8 GHz

Required frequency accuracy ~ 0.02 Hz

→ Relative accuracy ~ 2×10^{-12}

The stability of usual oscillators > 10^{-6}

Ultra-Stable Oscillator (USO) on Akatsuki

Stability of USO after the launch

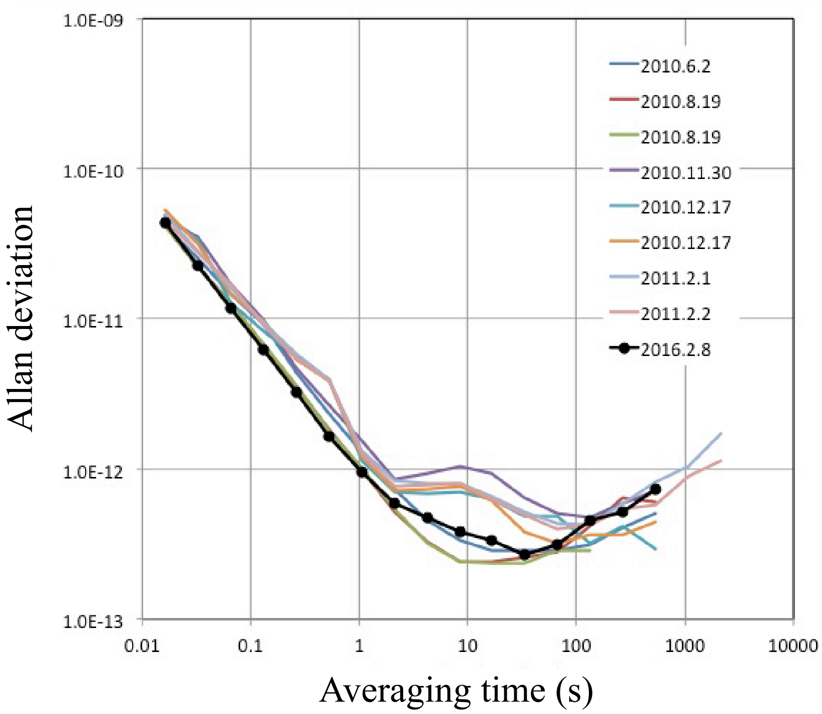

USO on Akatsuki

The requirement (Allan dev < 1×10^{-12} for τ = 1-1000 s) is satisfied.

Data acquisition

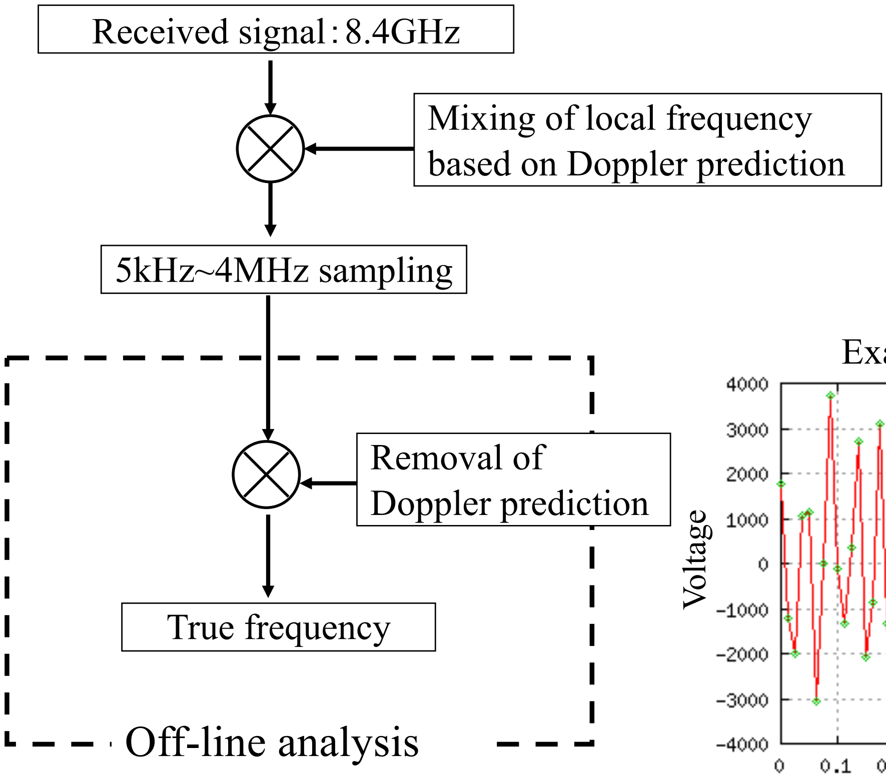

Usuda Deep Space Center (UDSC)

Example of raw data

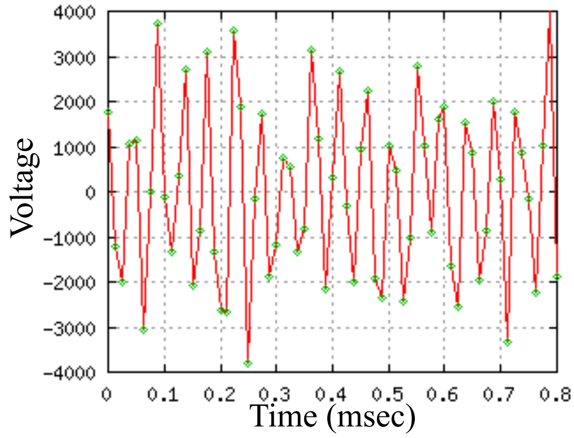

Raw data of radio wave from Venus orbiter Akatsuki

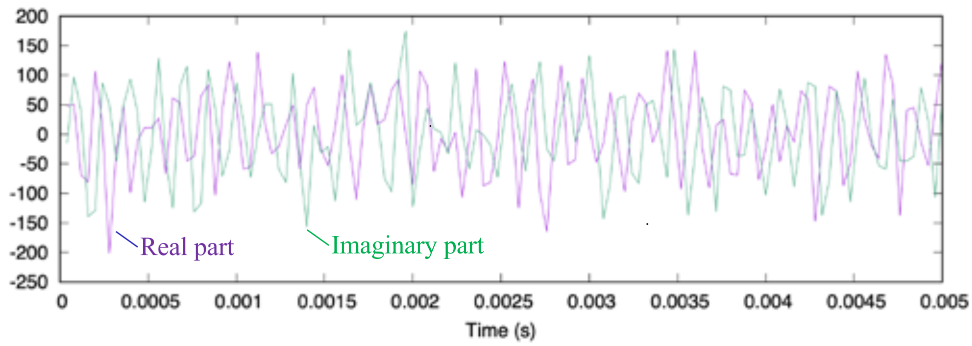

Signal spectrum

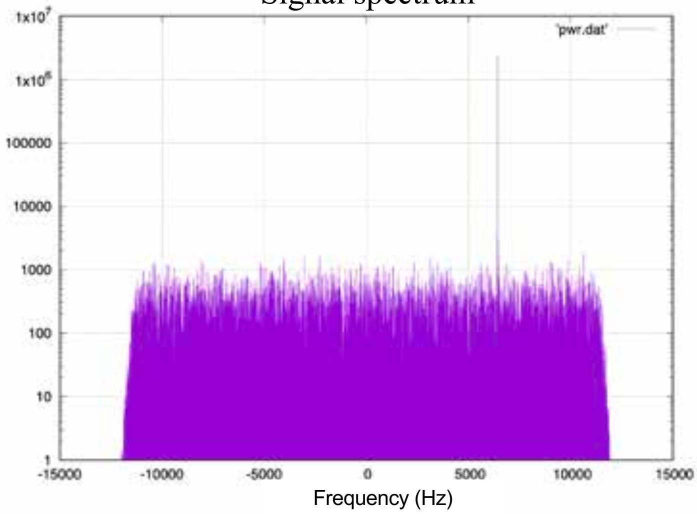

Required accuracy

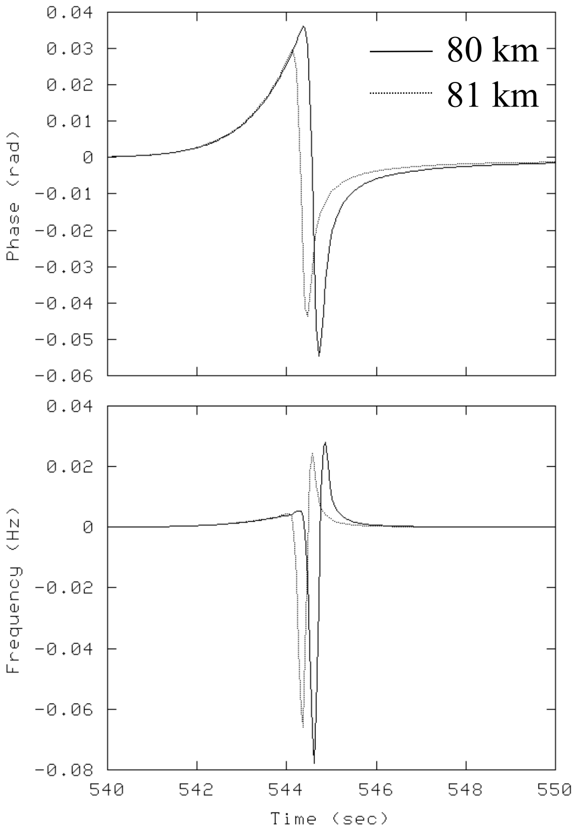

Change in phase/frequency caused by a Gaussian-type 0.2 K-perturbation with 1 km-thickness

Phase accuracy $\sigma_{rad} = 0.01$ rad
→ Required S/N ratio = $1/\sigma_{rad}^2 = 10000$

Need for narrow-band filtering (example from Akatsuki)

- Signal level at the receiver P = 3.0×10^{-17} W (at 1.73 x Earth-Sun-distance)
- Noise temperature of the receiver = 96 K (Usuda Deep Space Center)
  → kT ~ 1.3×10^{-21} (J = W/Hz)

Letting the band width B (Hz), the S/N ratio is given by

$$P/kTB \sim 2.3 \times 10^{-4}/B$$

So that the S/N ratio is higher than the required value of ~10000, we require

$$B < 20 \text{ Hz}$$

Usually the influence of the uncertainty in the orbital motion the transmit frequency is larger than this bandwidth. We must first stabilize the signal frequency.

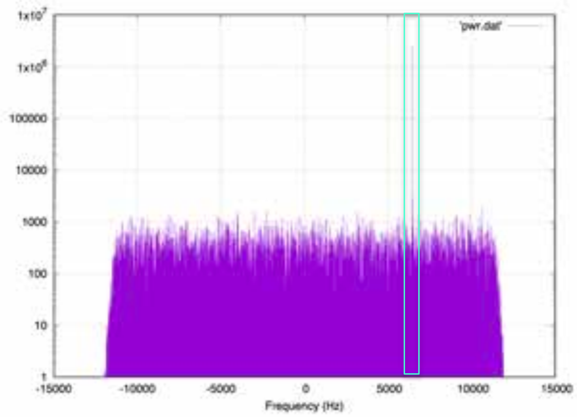

Frequency determination by FFT & spectral fitting

Successive FFTs for short segments

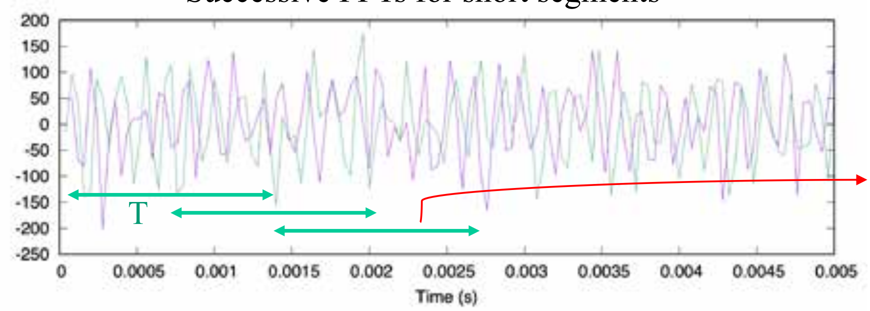

Fitting of Sinc function

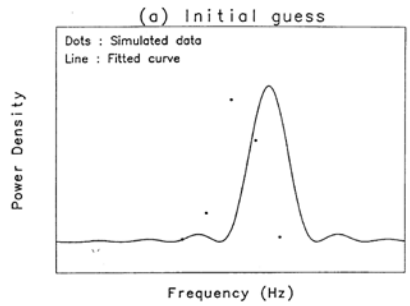

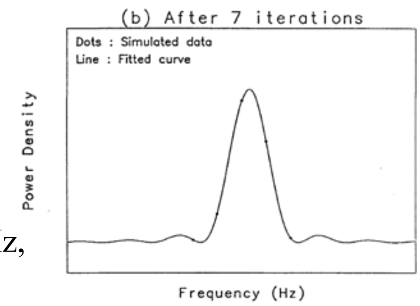

Frequency resolution of FFT

$$\Delta f = 1/T = 1/(\tau * N)$$
$$= 1 / ((1/B) * N)$$
$$= B/N$$

T : time interval of FFT
τ : sampling interval
N : FFT length
B : bandwidth = sampling frequency (for complex data)

For example, to achieve a frequency accuracy of $\Delta f = 0.02$ Hz, the time interval should be $T = 1/\Delta f = 50$ s.
(If the sampling frequency is B = 25 kHz, the FFT length is
$N = T/\tau = T/(1/B) = T*B = 1250000$)

Frequency determination by FFT & spectral fitting

Successive FFTs for short segments

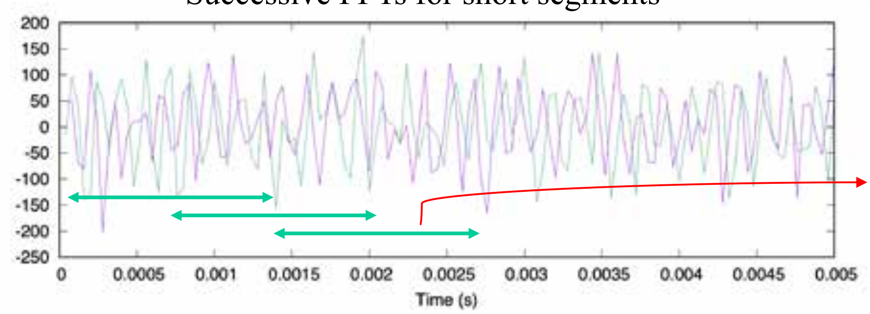

Fitting of Sinc function

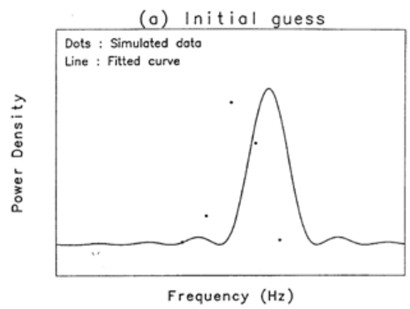

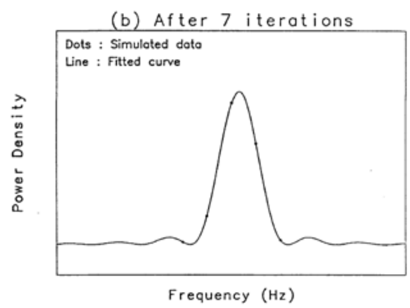

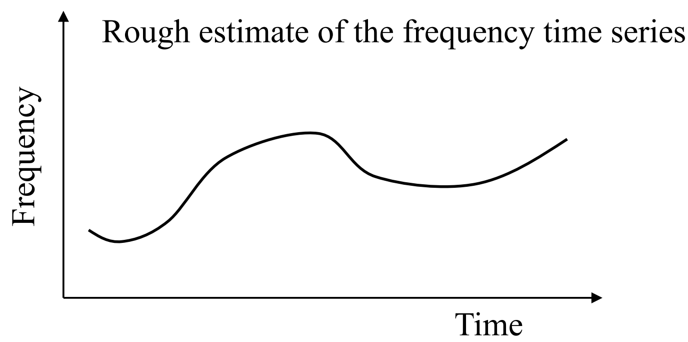

Extracting the roughly estimated frequency

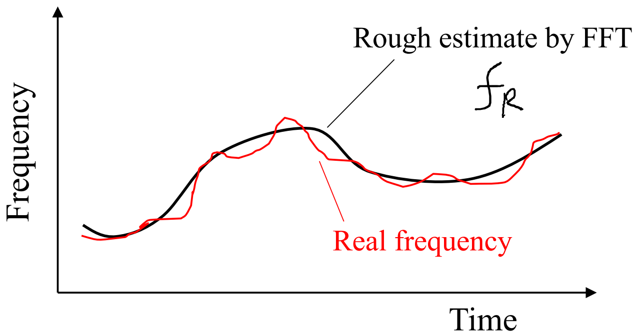

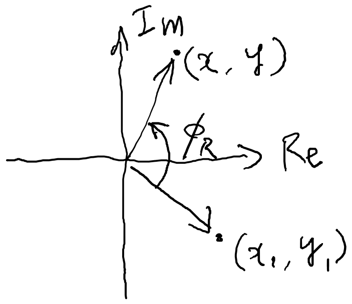

$$\phi_R = \int^t f_R(t')\,dt'$$

$$\begin{pmatrix} x_1(t) \\ y_1(t) \end{pmatrix} = \begin{pmatrix} \cos(-\phi_R) & -\sin(-\phi_R) \\ \sin(-\phi_R) & \cos(-\phi_R) \end{pmatrix} \begin{pmatrix} x(t) \\ y(t) \end{pmatrix}$$

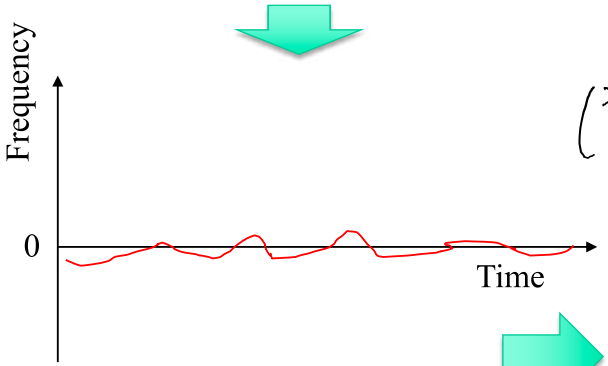

Narrow-band filtering

Filtering and decimation

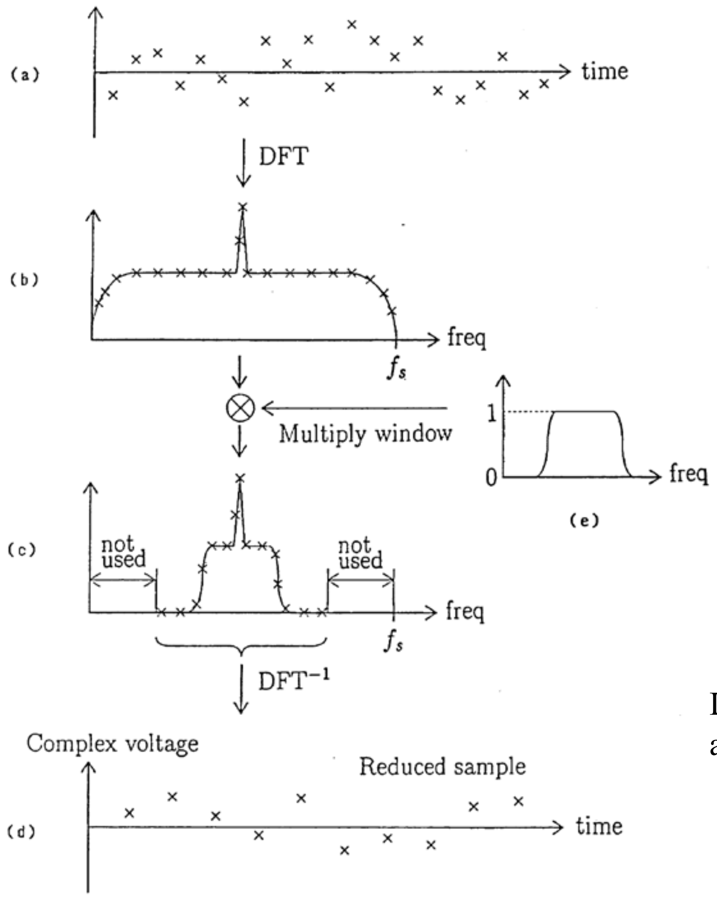

Low-noise data is created by arrow-band filtering

Phase unwrapping

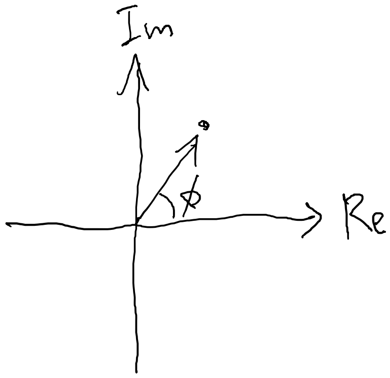

$$f = \frac{d\phi}{dt}$$

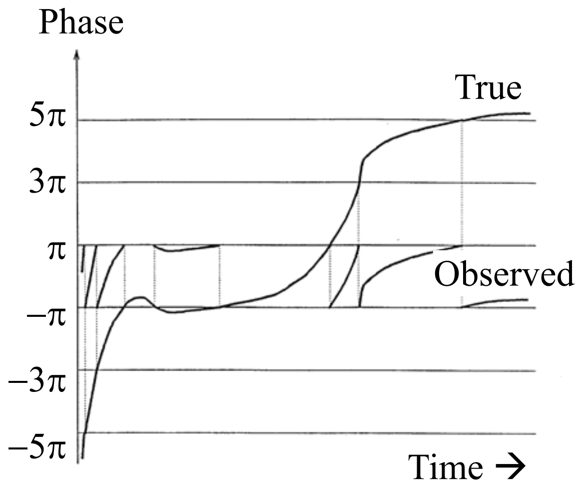

With sufficiently low-noise, the phase can be obtained from the real and imaginary components of the data at each time step. The frequency is obtained by differentiating the phase.

Radio occultation measurement

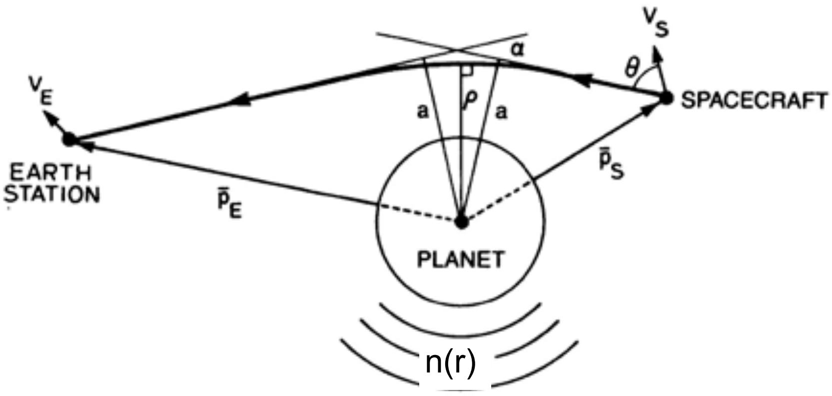

a : Impact parameter
α : Bending angle
n : Refractive index
r : Distance from planet center

Tyler (1987)

$$\alpha(a) = -2a \int_{r=r_0}^{r=\infty} \frac{1}{n} \frac{\partial n}{\partial r} \frac{dr}{\sqrt{(nr)^2 - a^2}}$$

Abel transformation:

$$\pi \ln n(r_{01}) = -\int_{a=a_1}^{a=\infty} \frac{\alpha(a)}{\sqrt{a^2 - a_1^2}}\, da$$

Refractive index n is related to atmospheric structure:

$$\mu(r) = (n(r)-1)\times 10^6 \qquad \text{: Refractivity}$$

$$= \underbrace{\boxed{\kappa N_n(r)}}_{\text{neutral atmosphere}} - \underbrace{\boxed{40.3\frac{N_e(r)}{f_0^2}\times 10^6}}_{\text{plasma}}$$

Retrieval of the neutral atmosphere's temperature based on hydrostatic equilibrium:

$$T(r) = \frac{N_n(r_{top})}{N_n(r)} T(r_{top}) + \frac{\overline{m}}{kN_n(r)} \int_r^{r_{top}} N_n(r')g(r')dr$$

- Temperature at the upper boundary should be given from empirical models. The effect of the upper boundary almost disappears 1-2 scale heights below the boundary.

Retrieval of a temperature profile

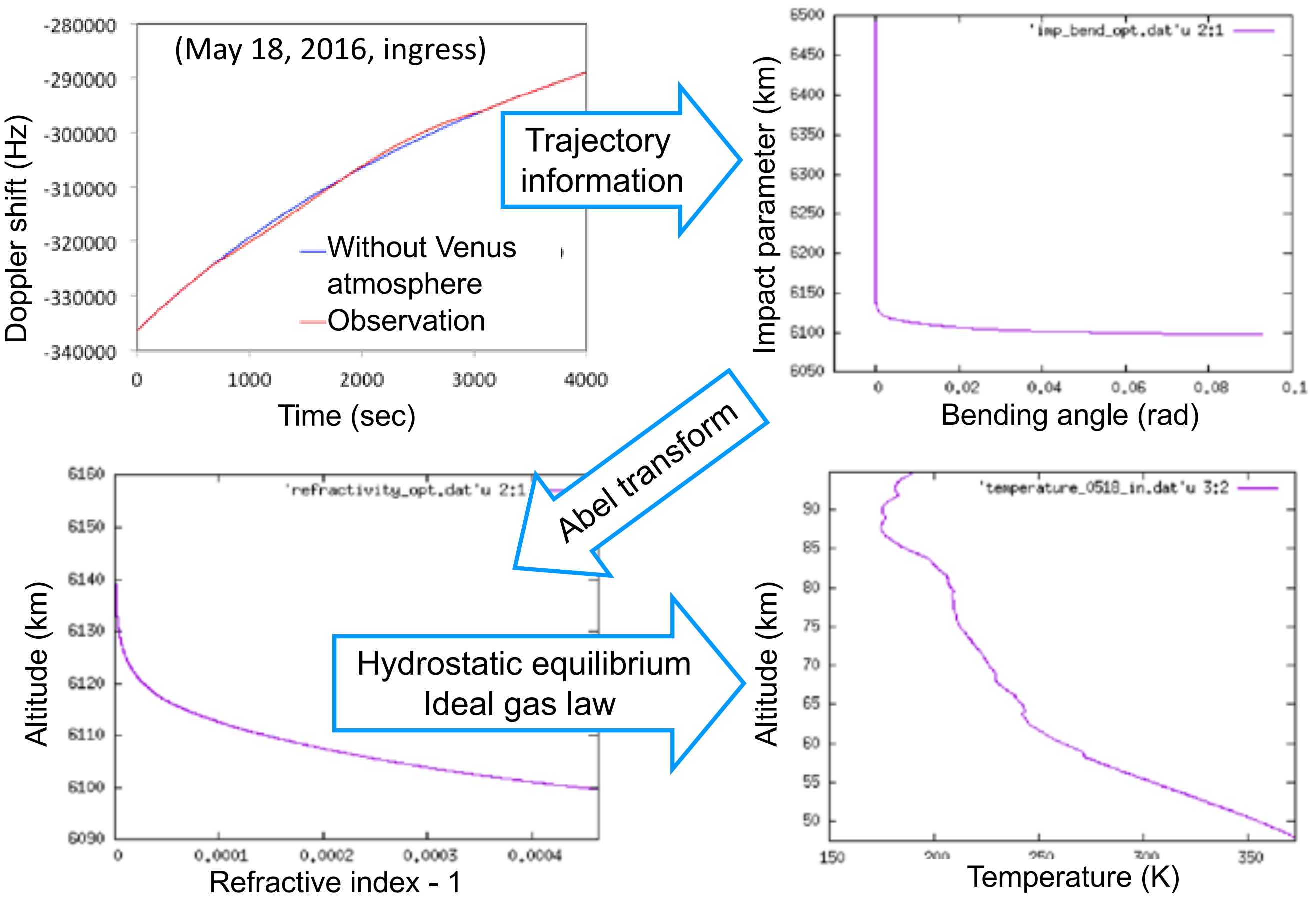

Temperature profiles of the Venus atmosphere obtained by Akatsuki radio occultation

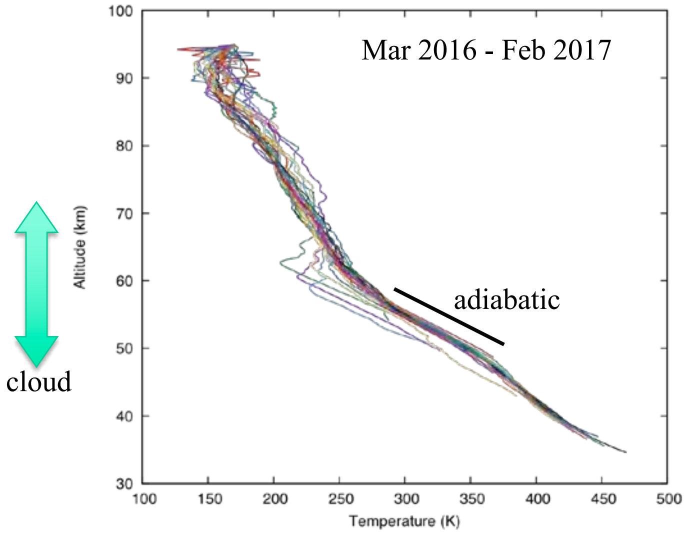

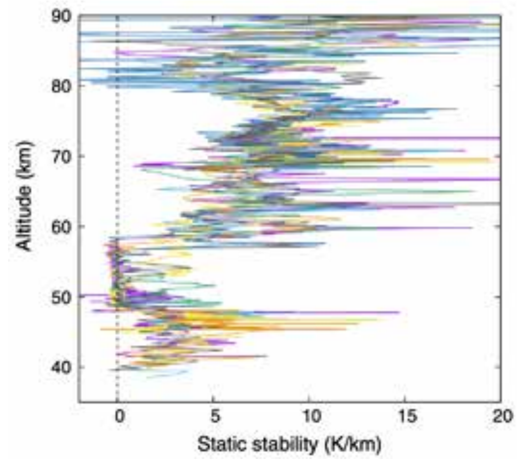

Imamura et al. 2017

static stability: $S = \frac{dT}{dz} - \frac{g}{c_p}$

T : temperature
z : altitude
g : gravitational acceleration
c_p : specific heat for constant pressure

Examples of Venus' electron density profile from Akatsuki radio occultation

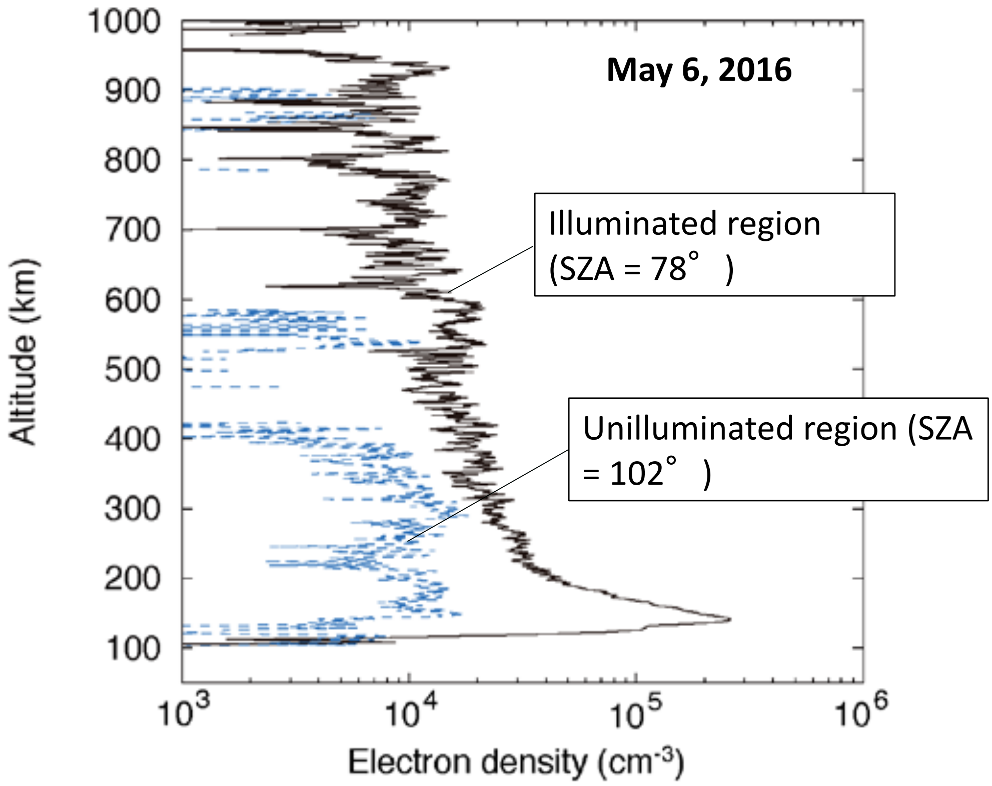

Accurate retrieval of phase difference between two signals

- The phase difference between right-circularly polarized (RCP) and left-circularly polarized (LCP) waves gives the Faraday rotation of the plane of polarization by magnetized plasma.
- Faraday rotation can be used to probe the magnetic field structure in the solar corona.
- The expected phase difference is of the order of 0.001 rad, which is difficult to measure for each wave due to large fluctuation of the received frequency.

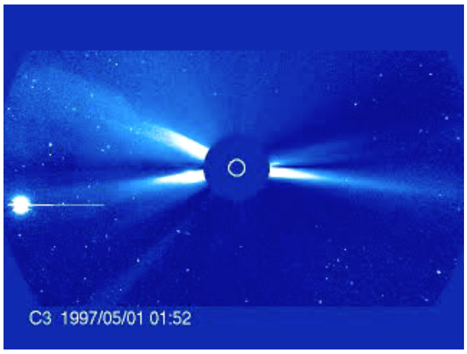

Derivation of the phase difference between RCP and LCP waves with cross-correlation analysis

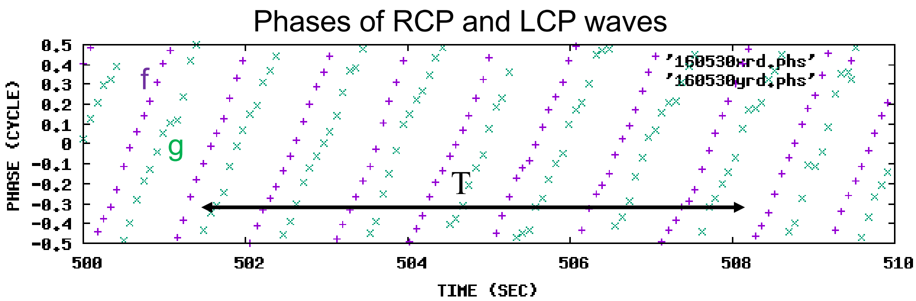

Cross-correlation

$$f \otimes g(\tau) = \int_{-T/2}^{T/2} f(t)\, g(t-\tau)\, dt$$

The phase difference is obtained from the time lag τ where the cross correlation peaks.

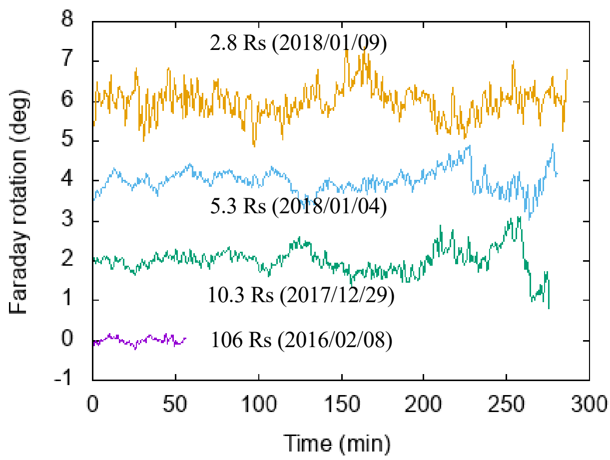

Doppler tracking of Juno spacecraft

- The spacecraft acts as a test particle falling in the gravity field of the planet. Jupiter's gravity is inferred from range-rate measurements between a ground antenna and the spacecraft during perijove passes.
- The ground station transmits two carrier signals, at 7,153 MHz (X band) and 34,315 MHz (Ka band). On board, an X-band transponder and a Ka-band frequency translator lock the incoming carrier signals and retransmit them back to the ground station at 8,404 MHz and 32,088 MHz, respectively. The range-rate (Doppler) observable is obtained by comparing the transmitted and received frequencies.
- Spherical harmonics representation of planetary gravity fields is determined by the density distribution inside the body.

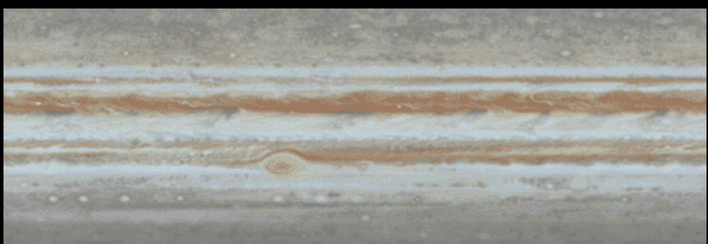

Doppler tracking of Juno spacecraft

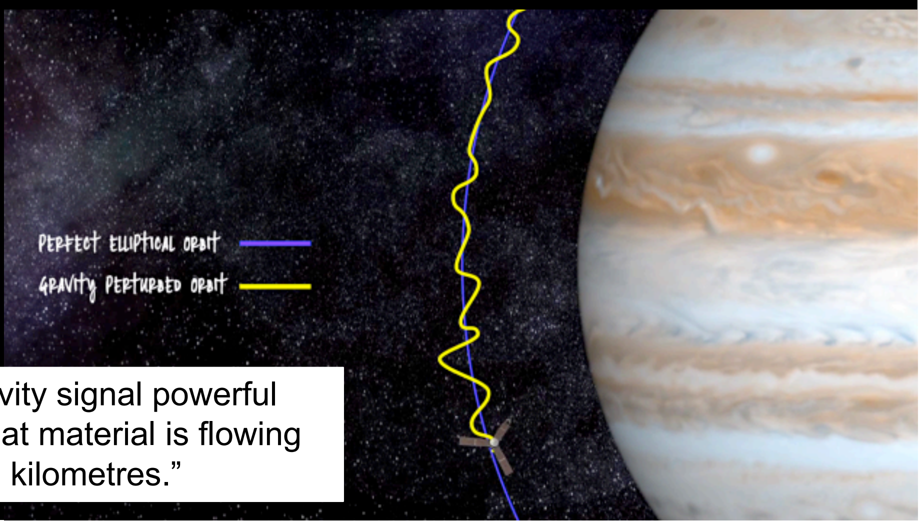

"Juno detected a gravity signal powerful enough to indicate that material is flowing as far down as 3,000 kilometres."

Less et al. (2018)

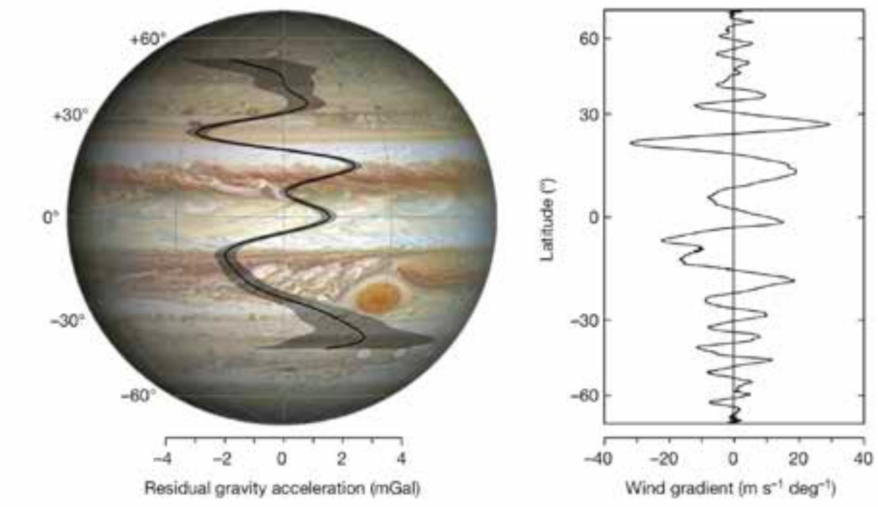

Figure 3 | Gravity disturbances due to atmospheric dynamics. a, An image of Jupiter taken by the Hubble Wide Field Camera in 2014 (https://en.wikipedia.org/wiki/Jupiter), showing the latitudinal dependence of residual gravity acceleration (in milligals, positive outwards) and associated 3σ uncertainty (shaded area) at a reference distance of 71,492 km, when the gravity from the even zonal harmonics J_2, J_4, J_6 and J_8 is removed. The residual gravity field, which is dominated by the dynamics of the flows, shows marked peaks correlated with the band structure. **b**, Latitudinal gradient of the measured wind profile. The largest (negative) peak of -3.4 ± 0.4 mGal (3σ) is found at a latitude of 24° N, where the latitudinal gradient of the wind speed reaches its largest value. The relation between the gravity disturbances and wind gradients is discussed in an accompanying paper[4].

"The observed jet streams, as they appear at the cloud level, extend down to depths of thousands of kilometres beneath the cloud level, probably to the region of magnetic dissipation at a depth of about 3,000 kilometres"

Planetary images

- The contrast in an original image is dominated by geometrical (illumination) effects. To visualize the detail of the surface, the effects need to be removed.

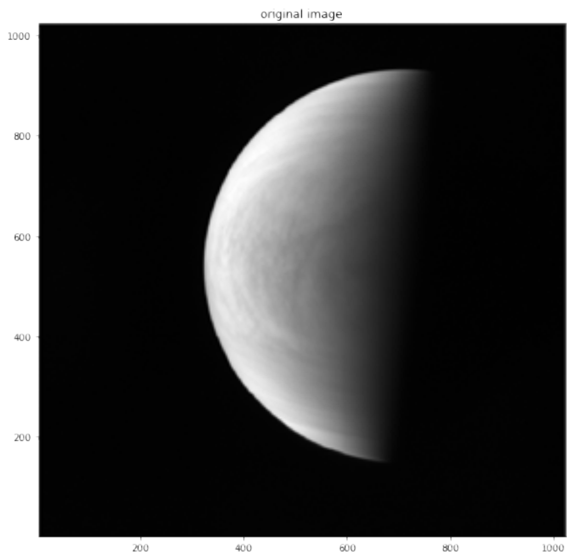

UV image of Venus taken by Akatsuki

Photometric correction

- The incident solar flux at each position on the planetary surface is proportional to the cosine of the incidence angle.
- The illumination effect can be roughly removed by dividing the original image by the model image, which is cosine of the incidence angle. (In real applications, more complicated model is used.)

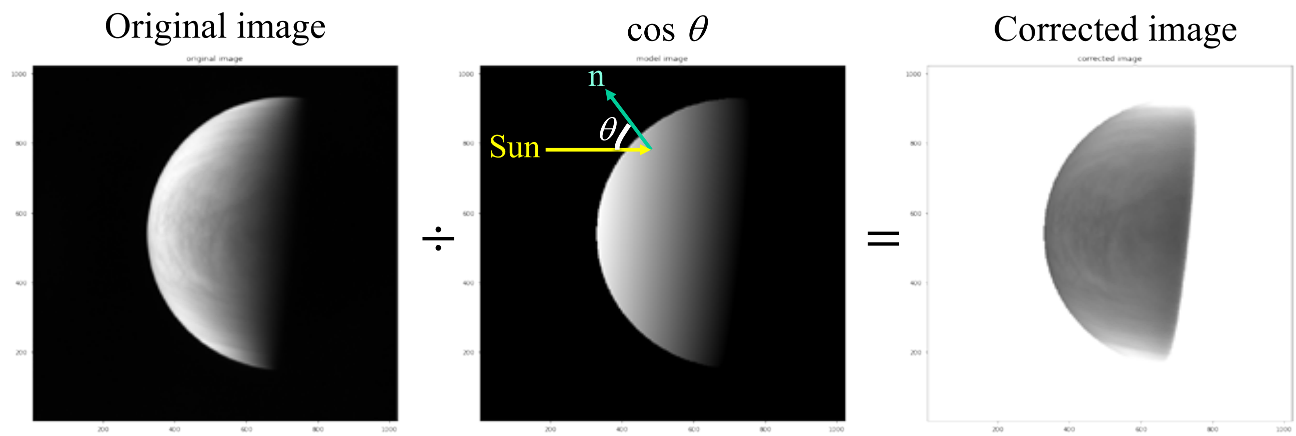

High-pass filtering

- To see the details of the surface, high-pass filtering is frequently used.
- High-pass filtering can be done by subtracting a smoothed image from the original (corrected) image. Moving average (running average) with a Gaussian function is frequently used for smoothing.

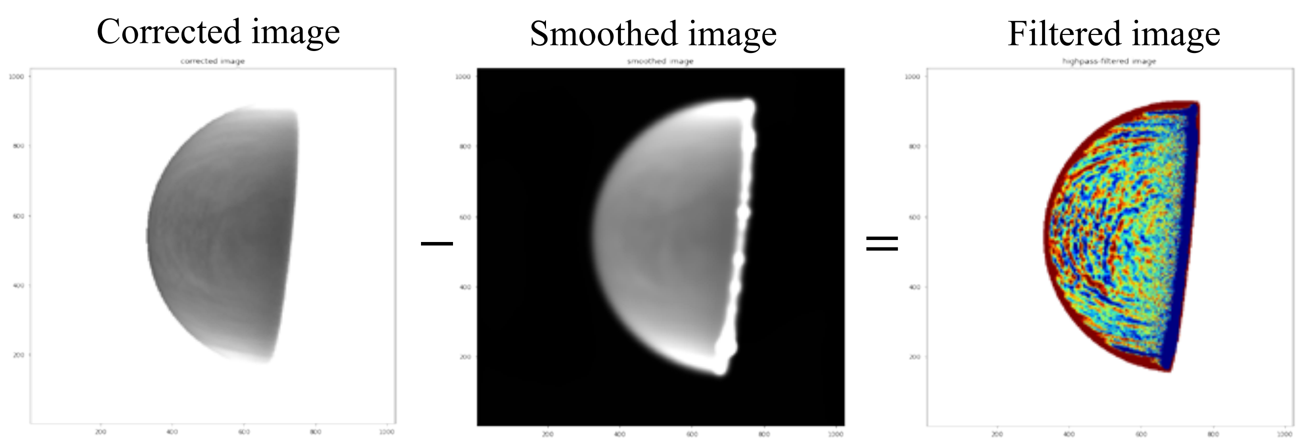

Projection onto planetary coordinate

- Movement of the atmosphere can be observed by projecting successive images onto the planetary coordinate.

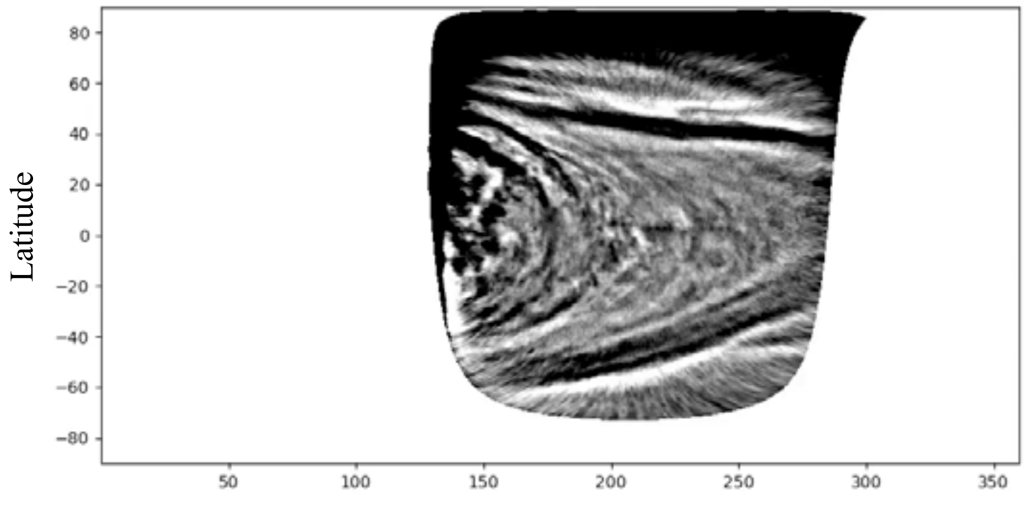

Cloud tracking

- Movement of the atmosphere can be observed by projecting successive images onto the planetary coordinate.

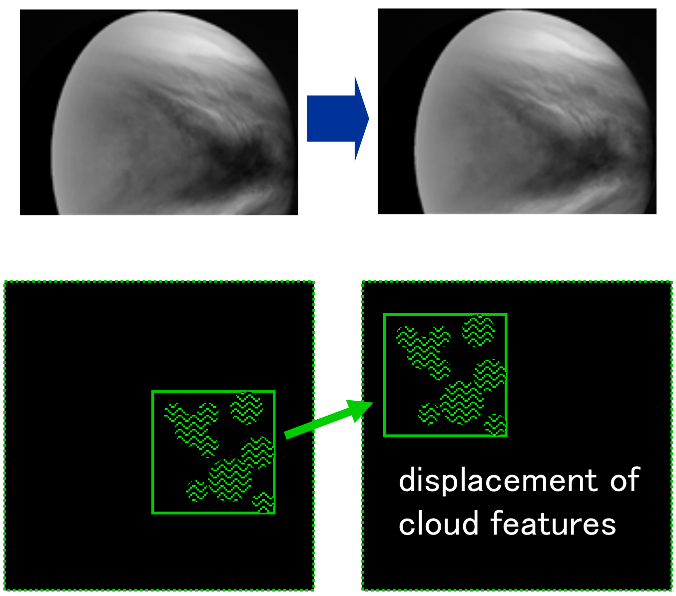

Cloud-tracked vectors (Nara, 2020)

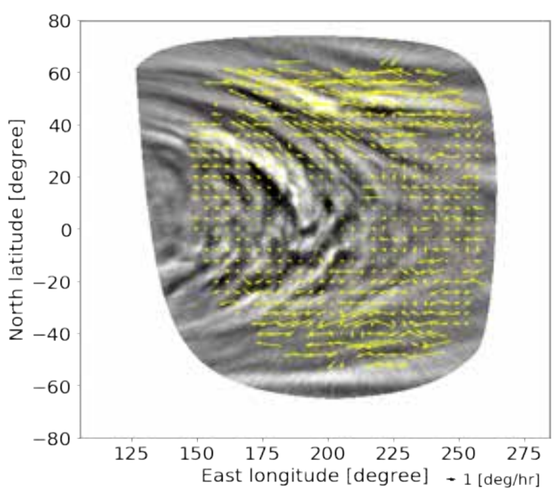

Cloud tracking with cross-correlation method

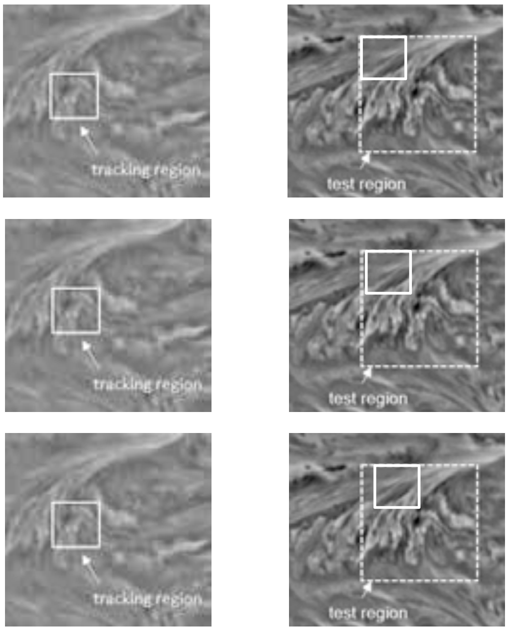

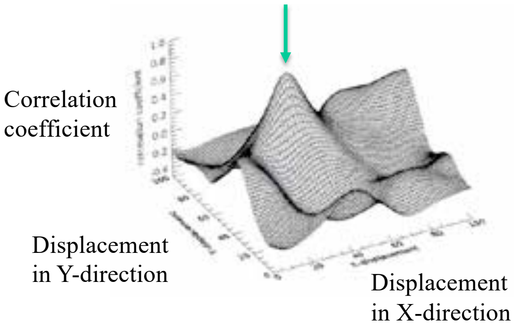

- The peak position on the correlation surface gives the displacement vector.
- Division the displacement by the time interval gives the velocity vector.

Superrotation of Venus' atmosphere

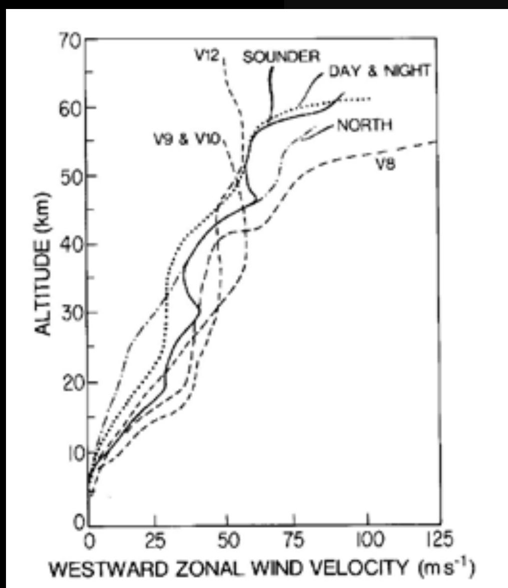

In-situ measurements of zonal winds (Schubert et al. 1980)

Zonal circulation at velocities 60 times faster than the solid surface

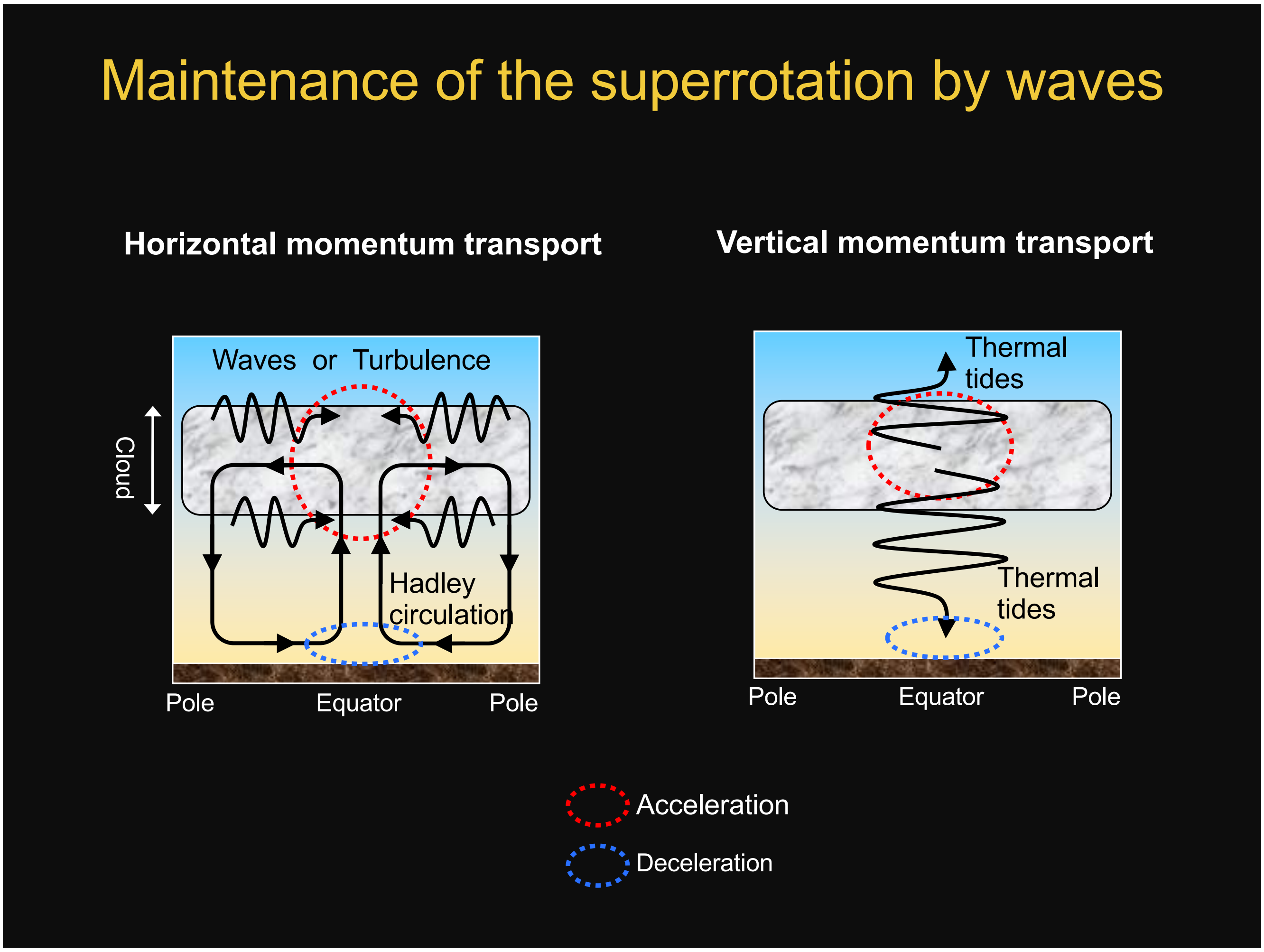

Tracking of faint cloud features in thermal infrared images

UV (283 nm) and thermal infrared (10 μm) images taken simultaneously by UVI and LIR (Fukuhara et al., 2017)

UV (283 nm)

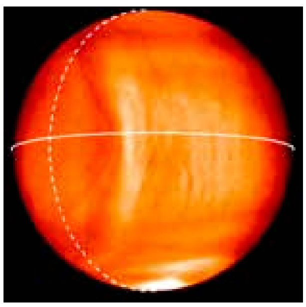

thermal infrared (10 μm)

Thermal infrared images allows observations of all local time regions

Characteristics of LIR data

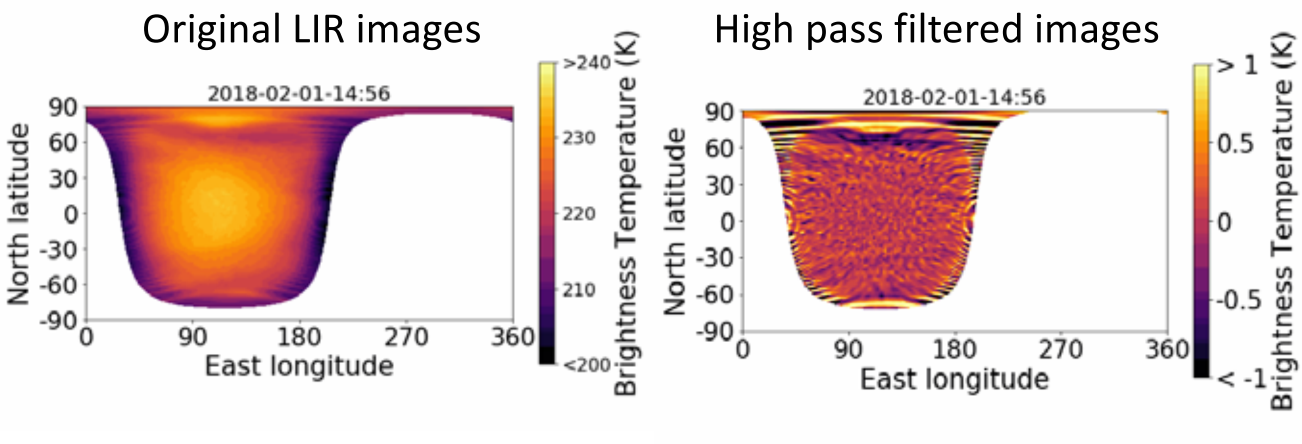

- Most of the small-scale cloud features have amplitudes comparable to or smaller than the LIR's temperature resolution of 0.3 K.
- Difficult to track cloud patterns in original images

Noise reduction by averaging images

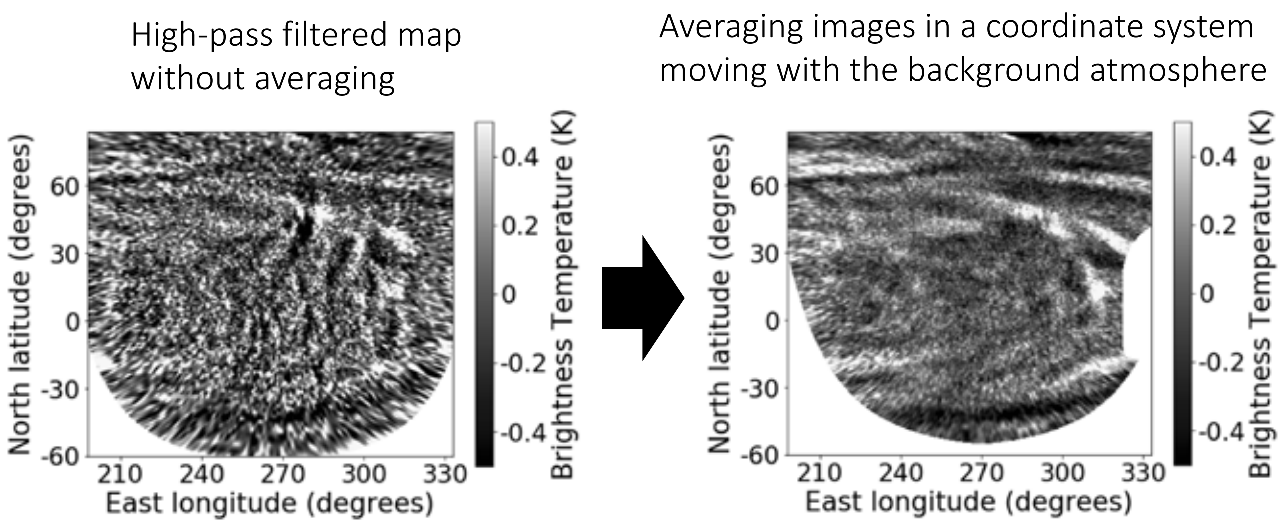

- Running-averaging of images in the time domain in a coordinate system moving with the superrotation
- S/N ratio is increased and topography-related features are smoothed out.

Moving features

Dayside

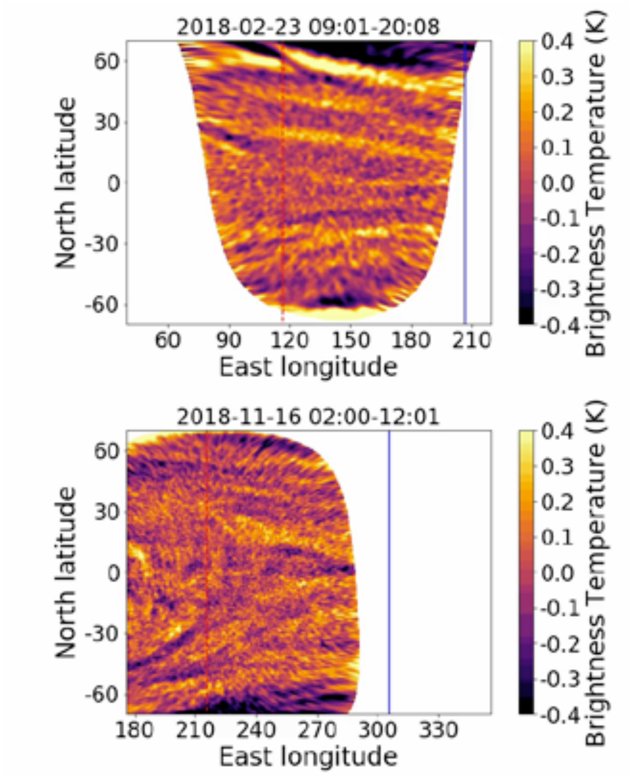

Nightside

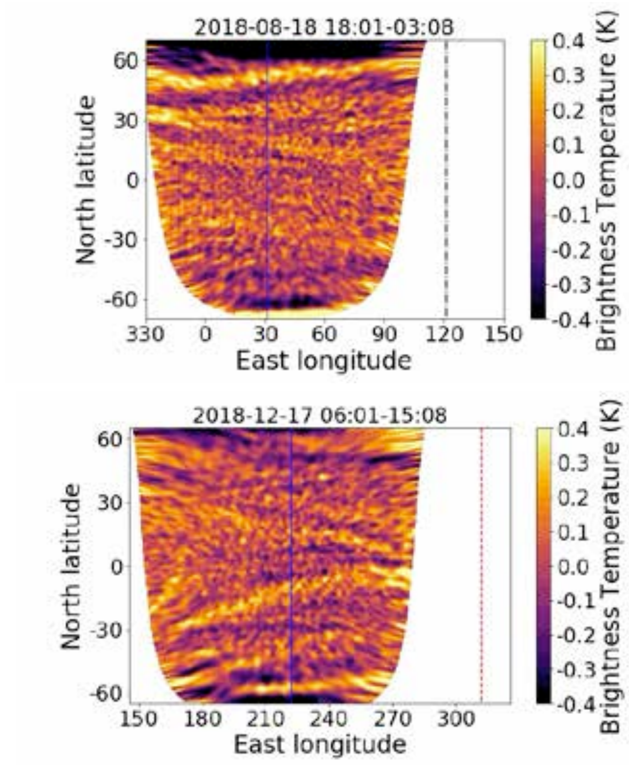

Local solar time-latitude distribution